Electronic Supplementary Material (ESI) for Environmental Science: Atmospheres.

Supplement for

A Conceptual model of northern midlatitude tropospheric ozone

Charles A. Mims,*[a] David D. Parrish [b], R. G. Derwent [c], Mohammad Astaneh[d] and Ian C. Faloona [d]

[a] Department of Chemical Engineering & Applied Chemistry, University of Toronto Ontario, Canada.

[b] David.D.Parrish, LLC, 4630 MacArthur Ln, Boulder, Colorado, USA.

[c] rdscientific, Newbury, Berkshire, UK.

[d] Department of Land, Air, & Water Resources, University of California, Davis, California, USA.

Contents of this file

Introduction

This supporting information presents additional analysis used in the main text:

Section S1 presents a calculation of ozone loss rate in the MBL from photolysis to (O^1D)

Section S2 derives MBL mixing rates from the contrast of ozone seasonal cycles measured in the MBL and the free troposphere

Section S3 discusses flexible function for fitting seasonal cycles.

Section S4 describes a simplified 3-box model.

Section S5 investigates contributions to the tropospheric ozone burden.

Section S6 presents an analysis of CASTNET continental surface ozone concentrations.

Section S7 describes a Monte Carlo uncertainty analysis

Section S8 discusses model simplifications and their likely impact

Section S9 gives examples of the use of this simple model in complex investigations

Section S1: Marine ozone photolytic loss parameters - seasonal variation

The major loss of ozone over the oceans is triggered by the photochemical process

$h\nu$ (<350 nm) + $O_3 \rightarrow O_2 + O(^1D)$		[S1]
$O(^1D) + H_2O \rightarrow 2\ OH$	$k_{298} = 2.2 \times 10^{-10}$ cm^3 molecule^{-1} s^{-1}	[S2]
$N_2 + O^1D \rightarrow O^3P + N_2$	$k_{298} = 3.1 \times 10^{-11}$ cm^3 molecule^{-1} s^{-1}	[S3]
$O_2 + O^1D \rightarrow O^3P + O_2$	$k_{298} = 3.95 \times 10^{-11}$ cm^3 molecule^{-1} s^{-1}	[S4]

and followed by subsequent steps of the HO_x cycle (Ayers et al., 1997). Competing processes for [S2] are deactivation collisions [S3] and [S4]. The rate constants indicated are from (Burkholder et al., 2019).

There is a strong seasonal variation in $J(O^1D)$, the UV photolysis frequency of step [S1], due to seasonal variation in solar zenith angle. The $O(^1D)$ deactivates to the ground state $O(^3P)$, which quickly reforms ozone, by collisions with gaseous species other than water vapor in reaction [S2]. The seasonal sea surface temperature (SST) cycle affects the atmospheric H_2O content, which affects the branching ratio to [S2]. The combination of the two factors introduces a strong seasonal variation in the ozone loss rate over the ocean. We attribute our $k_{B,m}$ to this process and here estimate its value and seasonal dependence based on this mechanism.

UV flux: The UV flux near the surface has a strong dependence on solar zenith angle - stronger than a cosine dependence due to UV absorption by the ozone layer above as well as scattering. Wilson (2015) measured the seasonal dependence of $JO(^1D)$ at Cape Grim (latitude 41°S) and analyzed the data using a transmitted UV formalism. We use the two-term functional fits to the median data in his Table 2 to calculate $JO(^1D)$ for other latitudes.

$$J\ (O^1D)\ (s^{-1}) = 4.2 \times 10^{-4} \exp(-2.7/\cos(z)) + 1.5 \times 10^{-5} \exp(-0.69/\cos(z)) \quad [S5]$$

This function (without the "radiation amplification factor" correction of Wilson (2015; p 7341) was integrated over the diurnal zenith angle profile at a range of latitudes and days of the year. The monthly averages from these results (shown in Figure S1), expressed in units of day^{-1} show the expected strong seasonal and latitude effects.

The annual variation ranges from a factor of ~4 at 30°N to over 10,000 at 60°N. Interestingly, the average over the entire latitude range has an annual variation of a factor of ~10, similar to the factor of ~12 measured at Cape Grim.

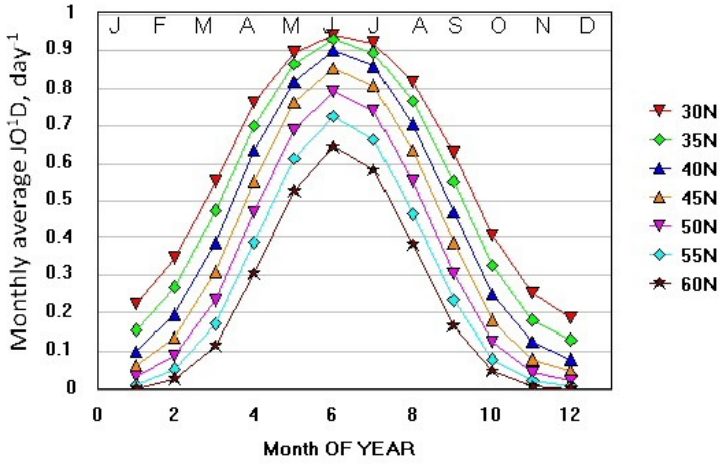

Figure S1: Monthly averaged values of JO^1D at various latitudes.

H_2O vapor concentration: The average ocean surface temperature (SST) varies annually by 8-10 C at mid-latitudes. This produces an approximate factor of 2 seasonal variation in the saturated H_2O vapor pressure in the marine boundary layer air above the ocean surface. The peak average water temperature lags the solar cycle by over 2 months, reaching a maximum in late August to early September, resulting in the northern hemisphere hurricane season. Average sea surface temperatures at 0.2m depth (Boyin et. al, 2017) as a function of latitude and season were derived from the GISTEMP v. 5 data shown in Figure S2 (GISTEMP, 2021; Lenssen et.al., 2019).

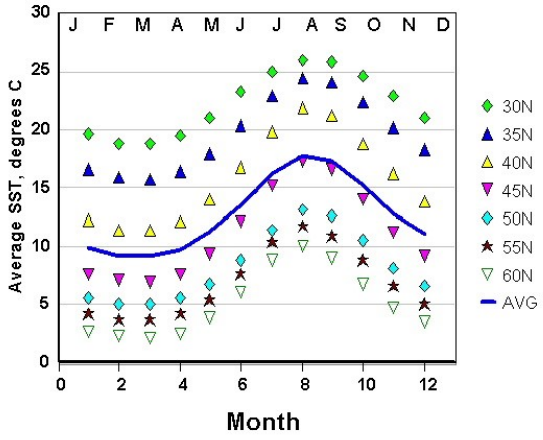

Figure S2: Calculated monthly average SST values at various northern latitudes.

At each latitude and month, the mole fraction of water in a saturated atmosphere was calculated from these temperatures. The branching ratio for reaction [S2] was then calculated using that mole fraction and the k_{298} values from Burkholder et al. (2019), then multiplied by the J (O^1D) values in Figure S2 to give the local $k_{B,m}$ shown in Figure S3.

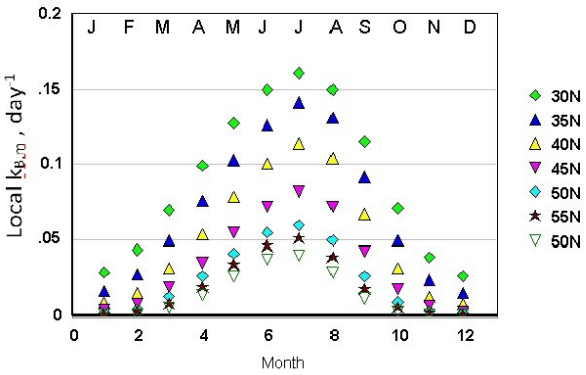

Figure S3: Calculated monthly average $k_{B,m}$ values at various northern latitudes.

These local values of $k_{B,m}$ were averaged over latitude to give the seasonal variation of the primary photochemical ozone destruction "rate constant", $k_{B,m}$, (symbols in Figure S4) with a maximum in July-August, delayed from the peak photochemical activity in June by the ocean temperature cycle. Finally, $k_{B,m}$ averaged over the year gives the value of $k_{B,m}$ of 0.051 day^{-1} corresponding to a lifetime of ~20 days, which is in reasonable accord with the ozone photochemical loss (~17 days) given at 1 km by Figure S1 of Parrish et al. (2021). A functional fit to these data, used in the model, is described in Supplement S3. In the model, this functional form is preserved, but the equation is scaled as needed to close the material balance.

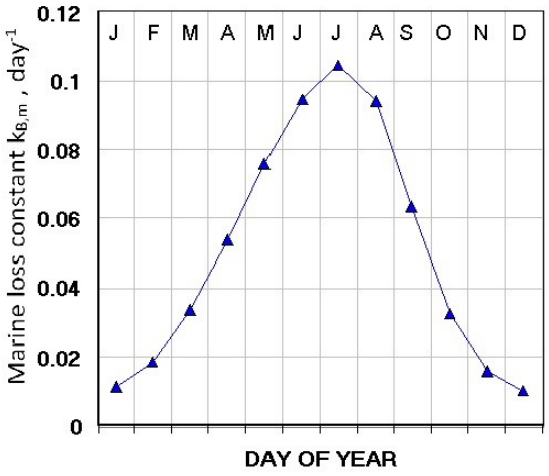

Figure S4: Calculated northern midlatitude (30-60N) averaged values of $k_{B,m}$ by month.

Section S2: Mixing parameters from FT and MBL ozone seasonal cycles

The seasonal dependence of the ozone loss rate in the marine boundary layer can be calculated directly from measured ozone seasonal cycles. Entrainment of air from the free troposphere (FT) is the predominant source of ozone to the marine boundary layer (MBL), yet the ozone seasonal cycle is very different in these two atmospheric layers; examples are given in Figure S5. This difference must arise from the seasonally dependent ozone loss rate in the MBL; here we use these two observed seasonal cycles as representative of their respective layers to derive a representative loss rate for the northern mid-latitude MBL. For the MBL, Eq. 1 of the text becomes

$$dX_B/dt = V_e/Z*(X_F - X_B) - k_{B,m}*X_B \qquad [S6]$$

where V_e is the entrainment velocity which equals Z/τ_B where Z is the MBL depth. Assuming steady state, algebraic manipulation gives the ozone concentration ratio

$$X_F/X_B = 1 + k_{B,m}*Z/V_e. \qquad [S7]$$

The last term of this equation calculated from the observed seasonal cycles is plotted as the gold curve in Figure S5. The grouping $k_{B,m}*Z/V_e$ is equivalent to $k_{B,m}*\tau_B$.

The blue curve is the seasonal cycle for $k_{B,m}$ calculated in the previous section. The similarity of the curve shapes is striking having been derived from entirely different perspectives, especially since many secondary issues are neglected, such as the seasonal cycles in Z, V_e, clouds, other losses and sources related to the photochemical cycles involving HO_2, NO_X, VOCs, possibly halogens, etc.

Nevertheless, assuming that the calculated value of $k_{B,m}$ is correct, and that Z and V_e remain constant over the seasons, the ratio of the gold to blue curves in Figure S5 gives the seasonal cycle of the MBL mixing time (τ_B; Figure S6). The annual average is 5.9 days, which for Z = 1 km corresponds to an entrainment velocity of 0.2 cm/s. The apparent seasonal variability of Z/V_e in Figure S6 is likely within the uncertainty of the analysis, but could possibly be interpreted as more rapid mixing between the MBL and FT in spring and autumn, compared to summer and winter. Since V_e drives the growth rate of the boundary layer, Z and V_e are very likely to be correlated.

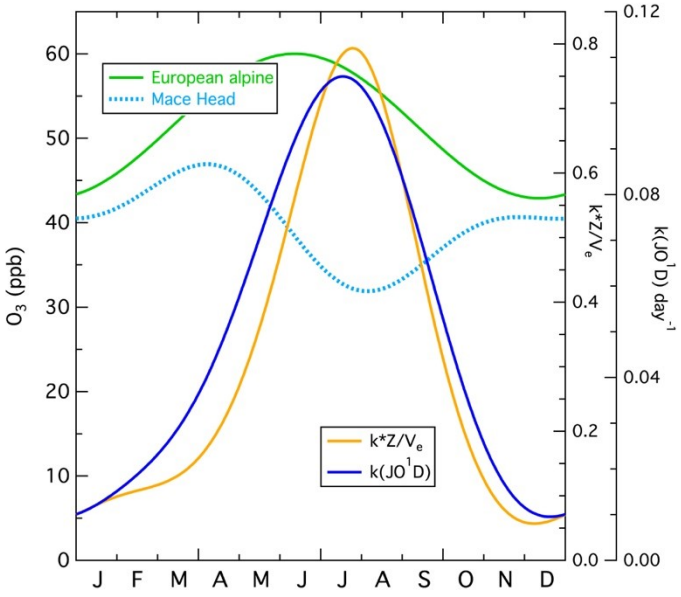

Figure S5: Comparison of ozone seasonal cycle at FT and MBL locations (green and blue dotted curves; Parrish et al., 2020). Dark blue curve gives the seasonal dependence of $k_{B,m}$ calculated from Eq. 10 of the text and plotted in Figure S4. Gold curve gives the ratio $k_{B,m}*Z/V_e$ derived from the seasonal cycles using eq. S7.

The MBL mixing parameters can also be derived from the observed MBL diurnal ozone cycle. On average the daytime loss of ozone must be balanced by entrainment of ozone from the FT. Ayers and Galbally (1995) present such an analysis for Cape Grim. They adopted a value of Z = 1 km based on a limited number of vertical ozone profiles measured in the vicinity of the site. Based on limited FT ozone

measurements and a seasonal mean ozone diurnal cycle derived from surface measurements, they derive an entrainment velocity of 0.35 ± 0.20 cm/s that agrees, within quoted uncertainties, with the result derived above. Later work by Ayers et al. (1997) selected a somewhat lower value of 0.3 cm/s.

For our base case simulation, we select the parameter values of Z = 1 km, V_e = 0.2 cm/s, and τ_B = 5.9 days derived from the seasonal cycle analysis. These are generally consistent with climatological references included in the paper. A discussion of the sensitivity of the model results to these parameters is included in the paper.

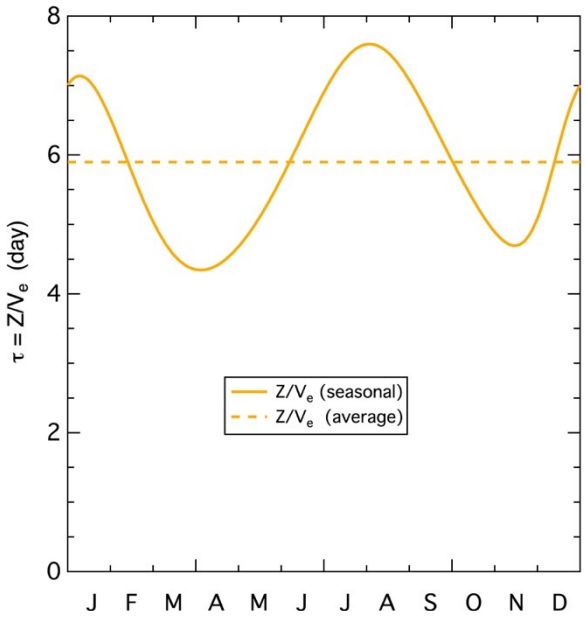

Figure S6: Ratio of boundary layer depth to entrainment velocity, which is τ_B of boundary layer mixing time.

Section S3: Functional fits for the time-dependent model:

The following general function:

$$F(\theta) = \langle F \rangle * \{A + B * ([\sin(\theta + \phi) + 1]/2)^n\} = \langle F \rangle * \{T(\theta)\} \qquad [S8]$$

produces a seasonal cycle with variable width, amplitude and phase. The annual average of parameter F, <F>, is multiplied by a unitless temporal function T(θ) representing the expanded expression inside the braces. Here, θ is the calendar day in radians and ϕ is a phase shift. T(θ varies between a minimum = A and a maximum = A+B; the exponent n adjusts the width of the seasonal cycle maximum; the A and B parameters are chosen so that the annual average of T(θ) equals unity.

The functions T(θ) used for the various model parameters described in the text are shown in Figure S7. The marine boundary layer losses were derived by the two different methods discussed in the preceding two sections: (1) based on the O^1D mechanism (Supplement S1) and (2) analysis of

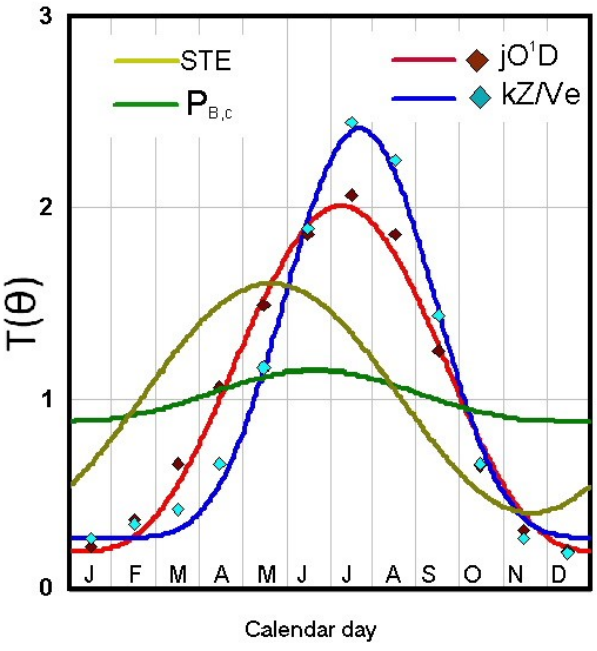

Fig. S7: Seasonal T(θ) functions used for the indicated parameters in the text. The scaled monthly data used for the two $k_{B,m}$ fits are also shown. The fit parameters are given in the manuscript.

the measured FT and MBL seasonal behavior (Supplement S2). The two functions have similar shapes (Figure S5) and were derived from monthly averaged data which are also shown in Figure S7 after scaling to give an annual average of 1.0. The functions used for the STE parameter and the continental source function for the simulation illustrated in Figure 7b are also shown. The equation parameters for these functions are given in the main body of the manuscript.

Section S4: Three-box model - sensitivity to marine boundary parameters:

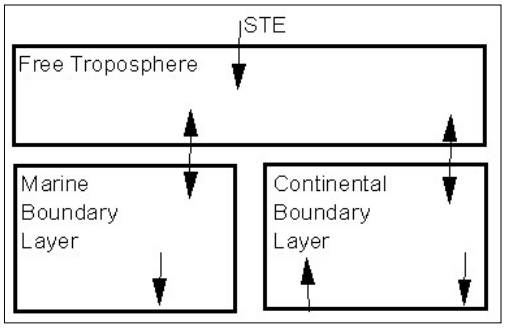

A simple 3-box model encapsulates the basic construct of the 18-box model and the "see-saw" relationship between the marine and continental boundary layers in simple algebraic form. The group of marine boundary layers is combined into one well-mixed compartment, the group of continental boundary layers into another, and the free troposphere layers into a third.

Steady state mass balance equations for each box are in units of ppb based on the entire northern midlatitude troposphere. The terms are defined similarly to those in the manuscript (but with simplified subscripts). Mixing times are based on the boundary layer boxes τ_M = mixing time for marine boundary layers, etc., and f_M, f_C are the fractions of the total troposphere included in the respective boundary layers; $f_M = 0.5*h_M$ and $f_C = 0.5*h_C$, since marine and continental segments each account for half of the longitudinal coverage. h_M and h_C are the column mass fractions derived from the respective BL heights.

Steady-state mass balances are given for the three boxes by (parameters defined similarly to the text):

Free troposphere: $0 = STE - (X_T-X_M)*f_M/\tau_M - (X_T-X_C)*f_C/\tau_C$ [S-9]

Marine boundary layers: $0 = (X_T-X_M)*f_M/\tau_M - k_M*X_M*f_M$ [S-10]

Continental boundary layers: $0 = (X_T-X_C)*f_C/\tau_C + P_C*f_C - k_C*X_C*f_C$ [S-11]

Equation [S-9] can be expressed as $STE = C + M$ [S-12]

where $C = (X_T-X_C)*f_C/\tau_C$, the continental mixing term, and $M = (X_T-X_M)*f_M/\tau_M$, the marine mixing term. Equation S-12 explicitly shows that total STE must equal the sum of the net ozone entrained into the continental and marine boundary layers. We define $R_M = M/STE$ as the fraction of STE removed by the marine layers; R_M is the variable plotted on the abscissas of Figures 3 and 4 of the text. If f_M, f_C, STE, X_M , X_T, τ_C, τ_M are fixed, numerical values for X_C, k_C and k_M (the variables plotted on the ordinates of Figures 3 and 4) can be calculated as a function of R_M.

Equation S-9 and the definition of R_M gives:

$$X_C = X_T - STE*(1- R_M)*\tau_C/f_C. \quad [S-13]$$

Substituting Equation S-13 into Equation S-11 and rearranging yields the following expression for k_C:

$$k_C = [STE*(1- R_M)/f_C + P_C]/X_C. \quad [S-14]$$

The value k_M can be calculated directly from Equation S-10 by replacing the first term by $STE*R_M$ and rearranging:

$$k_M = STE*R_M/(X_M*f_M). \quad [S\text{-}15]$$

Section S5: Stratospheric contribution to the tropospheric ozone burden.

The relative contributions of the stratosphere and the continental photochemical production (PCB) to the ozone burden can be evaluated within this model, since all non-linear aspects of the ozone budget are placed into the first order loss terms in the BL compartments; the model then consists of a system of linear equations. As such, the contribution of each source to the burden of ozone in each compartment is mathematically separable. The model results under the conditions of the seasonal cycle base case (Figure 6 in the text) with the PCB and STE sources turned off are shown in Figures S9 and S10, respectively, revealing the contributions of STE and PCB to the various compartments.

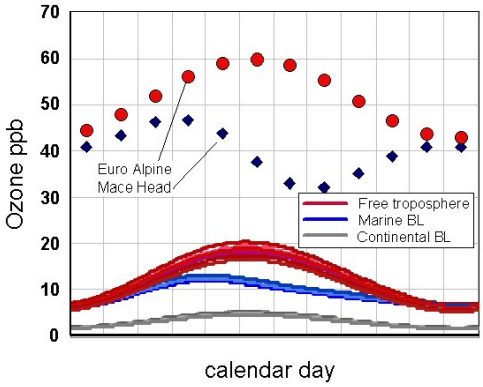

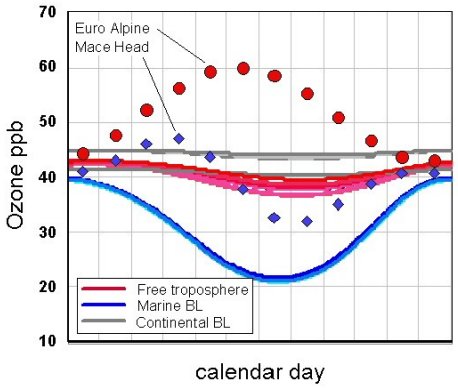

Fig. S8: (left) Base case time-dependent simulation with continental sources turned off, revealing STE contributions to compartmental burdens. **Fig. S9:** (right) Base-case time-dependent simulation with STE flux turned off, revealing contributions of continental sources to compartmental burdens.

The continental sources are responsible for the majority of the ozone burden in all the compartments. This is expected given the much larger (a factor of 12.8) amount of ozone generated annually in the continental boundary layers compared to STE. Averaged over the entire northern midlatitudes, however, the continental boundary layers contribute only 3.6 times the annual burden contributed by STE, which thus contributes ~ 3 times more ozone than expected from relative source strengths. Breakdown of this impact is summarized in the following table. This seasonal nature of this behaviour is clear in the Figures above. STE contributes up to one third of the marine boundary layer burden during mid-late summer.

Table S1: Ozone burden distribution, annually averaged, from the "base case" results shown in Figure 6 in the text.

	Annual Average Ozone Burden Contribution, ppb				**SOURCE, ppb/day**
Delivered to: ->	Free troposphere	Continental BL	Marine BL	Troposphere total	Troposphere total
FROM STE	10.2	0.33	0.64	11.2	0.40
FROM PBC	33.2	4.5	2.1	39.9	5.5
STE percentage	23.5%	6.8%	23.2%	21.9%	7.3%

Section S6: Ozone seasonal cycle in the US continental boundary layer

In the US, EPA's Clean Air Status and Trends Network (CASTNET- https://www.epa.gov/castnet) measures ozone at relatively isolated rural sites throughout the country. Here we use the data from many of those sites over the past ~30 years to estimate the ozone seasonal cycle in the US continental boundary layer. We base our analysis of the archived maximum daily 8-hour averages (MDA8s), as they are representative of the ozone concentration through the full depth of the continental boundary layer, since they generally occur during midday, when the convective boundary layer is fully developed. All available MDA8 were downloaded for all days at the selected sites from the CASTNET data archive (https://java.epa.gov/castnet/clearsession.do - last accessed 6 December 2021). Following the

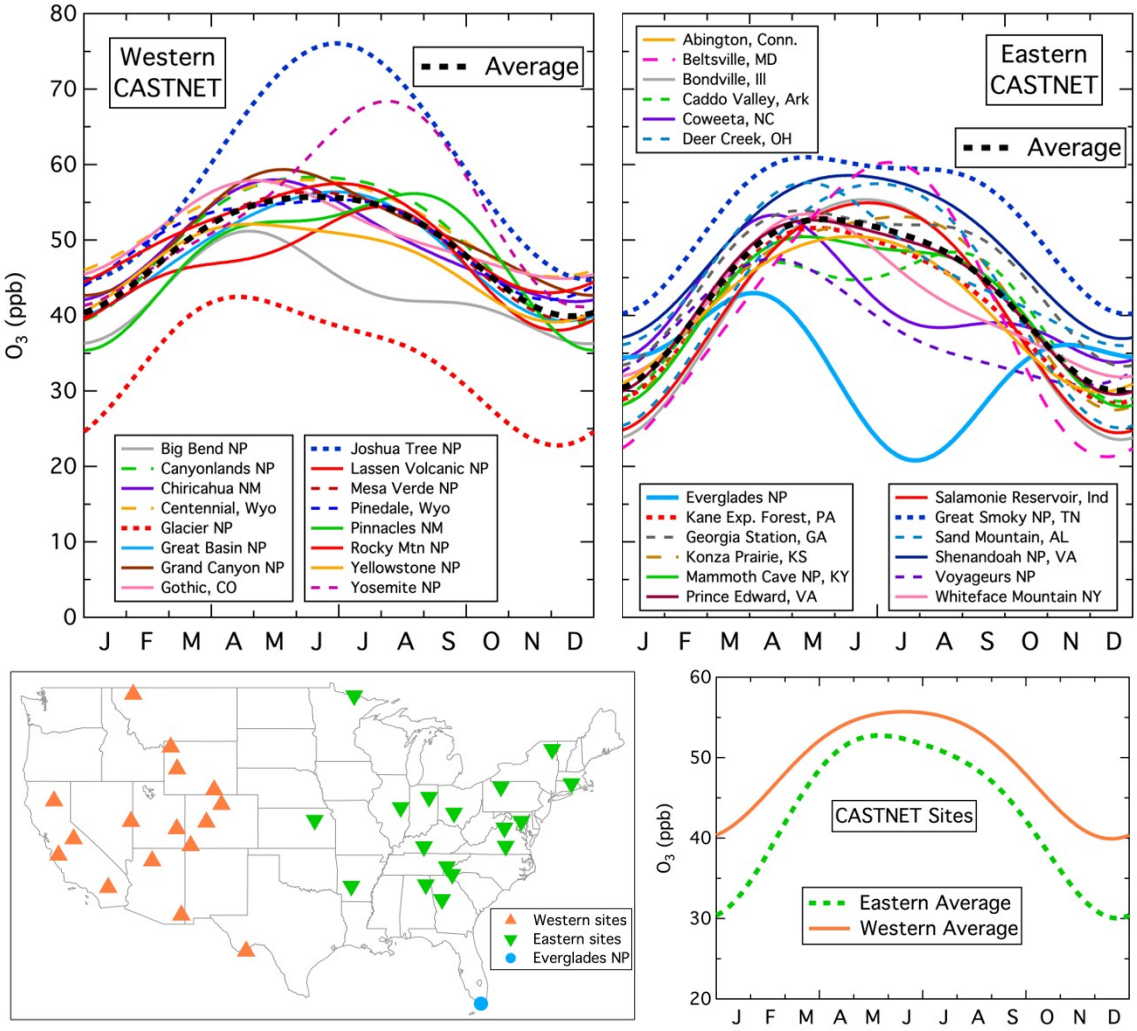

Fig. S10: Estimated ozone seasonal cycle in the US continental boundary layer. The map indicates the locations of selected CASTNET sites; 16 and 18 in the western and eastern parts of the country, respectively. The upper two graphs show the seasonal cycles derived from individual sites in the west (left) and the east (right), and averages of those individual seasonal cycles. The lower graph compares the two average seasonal cycles.

procedure of Parrish et al. (2019), the monthly mean MDA8 values were calculated for each site; these were detrended to remove long-term changes in the mean concentrations. Fourier transform analysis indicated that the fundamental (i.e., one sine cycle/yr) dominated the seasonal cycle at all sites with significant contributions from the second harmonic (i.e., two sine cycles/yr) at most sites. Higher order harmonics gave less significant contributions at some sites, but these were generally small. The curves in the two upper graphs of Figure S10 indicate the sum of the mean ozone concentration plus the fundamental and second harmonics of the seasonal cycle at each site. The illustrated seasonal cycles represent the mean seasonal cycle over the entire measurement record; at some sites the magnitude of the seasonal cycle has decreased significantly over the measurement record.

The seasonal cycles at almost all of the selected CASTNET sites are similar, with maxima in summer and minima in winter. Means of the individual sites are shown for each region. The results are similar between the western and eastern parts of the country; the mean is higher in the west, but both regional means are within the site-to-site variability in both parts of the country. In both regions there is an indication of lower concentrations to the south (Big Bend NP in the west, and Everglades NP in the east) and to the north (Glacier NP in the west, and Voyageurs NP in the east) with higher concentrations in a belt across the central part of the country, which is broadly consistent with satellite and modelling studies across the entire northern midlatitudes (e.g., Ziemke et al., 2011; Kerr et al., 2020). The highest concentrations are seen in the west, downwind of major pollution sources (Joshua Tree NP downwind of the Los Angeles Basin, and Yosemite NP downwind of California's San Joaquin Valley).

The Everglades NP site is the one site with clearly different behavior. It is located on the southern tip of Florida, outside of the northern mid-latitudes (25.4°N latitude). Its seasonal cycle has a clear MBL signature (compare with the Mace Head, Ireland seasonal cycle in Figs. 6 and 7 of the manuscript). Due to these differences the Everglades NP result in Figure S10 is excluded from the Eastern US average.

Section S7: Monte Carlo uncertainty analysis

The aim of this study has been to develop a simplified representation of tropospheric ozone sources, sinks and transport so that we can understand their representation within the highly complex earth system models used in climate policy support. However, one of the challenges of simple representations of complex processes is to ensure that the simplified parameters are reliable representations of the complex system and that no instabilities in the mathematics produce unacceptable uncertainty in derived parameter values. To this end, we have conducted a Monte Carlo uncertainty analysis.

A 3-step Monte Carlo assessment of the uncertainties in our continuous stirred tank reactor (CSTR) model was conducted. First, the same CSTR model code was used with one change - dry deposition over the continents was separated from the first order decay constant. As noted in the manuscript these two terms combine into an overarching first order loss process and has no effect on the conclusions here. The code was further altered to accept a multiplier for each model input parameter, scaling 'best estimate' parameter values given in Table 1 of the text; these multipliers defined an uncertainty range for each parameter. Second, these uncertainty ranges were sampled quasi-randomly to give input parameter values for initialization of a given CSTR model run. Third, a large number of model runs were conducted, each with a different quasi-random selection of input parameters. Each run returned the average free tropospheric and marine boundary layer mixing ratios of ozone with two tracers that labelled the origin of the ozone – either from the stratosphere or photochemical production in the continental boundary layer. In addition, model outputs were calculated for the mean tropospheric ozone column density and the mean ozone turnover time, calculated from the total model burden divided by the total ozone loss flux.

A total of eight CSTR input parameters were selected for Monte Carlo uncertainty analysis. Details of these parameters are given in Table S.2. For each of the eight input parameters, an estimated $3 - \sigma$ confidence range was established based on multiplicative scaling by a factor of between 0.65 and 1.35, that is, by just over a factor of two from maximum to minimum. The probability distribution within that range was taken to be a uniform distribution on either side of the 'Best Estimate', that is to say, a 'top-hat' in shape.

Having set the CSTR parameter value ranges for the eight input parameters, each uncertainty range was sampled quasi-randomly for each CSTR run. The CSTR model was then run 10,000 times, with each run having a different set of inputs. Each run generated different average free troposphere and marine boundary layer ozone mixing ratios, tropospheric column density, and the mean ozone turnover time. Inspection of the frequency distributions of the free tropospheric and marine boundary mixing ratios over the 10,000 runs revealed that they were implausibly wide. Although the uncertainty ranges of the input parameters appeared plausible, this was not apparently the case for the output results. This is illustrated in Figure S11 which presents the frequency distribution of the free tropospheric ozone mixing ratios. Inspection of this figure reveals an implausible range in predictions that spans from 12 ppb to over 100 ppb. This indicates that the observed mixing ratios to be matched provide a discerning filter for the acceptable range of input parameter values. An 'acceptable' range was therefore chosen for the output free tropospheric and marine boundary layer mixing ratios and only the sets of CSTR input

parameters that gave 'acceptable' mixing ratios were used in the following analyses . The 'acceptable' mean annual mixing ratios for the free troposphere were set between 47 and 57 ppb, whereas those for the marine boundary layer were between 34 and 44 ppb. These ranges are subjective; they are $\pm$ 5 ppb, which respectively include all north Atlantic MBL sites investigated by Parrish et al. (2016) and the northern midlatitude baseline sites free troposphere sites studied by Parrish et al. (2020). Of the 10,000 Monte Carlo runs, only 587 (i.e., ~6%) gave 'acceptable' free tropospheric and marine boundary mixing ratios.

Table S3 summarizes the outputs, together with their means and 2 – σ confidence intervals, for the 587 'acceptable' Monte Carlo replicates. These can be seen to cluster around the values recommended in the manuscript, indicating that the CSTR model does converge to physically realistic behavior. The modeled tropospheric ozone column density was 36.4 ± 3.6 DU, which compares closely with the observed value of 34.0 DU for 25^o N to 60^{o}N from the OMI/MLS satellite data of Ziemke et al. (2011). The CSTR model indicates that of the ozone present in the marine boundary layer, 6.7 ppb (i.e., ~18 %) and 31.1 ppb are of stratospheric and continental boundary layer origins, respectively, demonstrating the dominating influence of in situ tropospheric ozone production over stratosphere-troposphere exchange. The CSTR model somewhat underestimates the annual average mixing ratio of ozone of stratospheric origins, 6.7 ± 3.0 ppb, compared to that predicted by Lelieveld and Dentener (2000) for the Mace Head, Ireland monitoring station (10 ppb). The CSTR analysis based on the seasonal cycle (see Section S5) estimates a somewhat larger STE contribution (9 ppb) to the MBL. Given the uncertainties in these model analyses, this is very good agreement indeed.

To understand how the uncertainties in each of the eight model input parameters contributed to the uncertainty in a particular model output, multiple linear regression techniques were applied to the outputs from the Monte Carlo replicates. The data set employed in these regression analyses were the model outputs: free troposphere and marine boundary layer ozone mixing ratios, the mean tropospheric ozone column densities (TOCD) and the mean ozone turnover time, and the values of the eight scaling parameters, $p_1 - p_8$, employed in each CSTR run. Multiple linear regression was then used to express the outputs, such as TOCD, as functions of the input parameters using an equation of the form:

$$TOCD = a_1p_1 + a_2p_2 + \ldots + a_8p_8 \qquad (S16)$$

where $a_1 - a_8$ represent the slopes of the regression. Much of the analysis presented here used the partial correlation coefficients, R_{1-8} , of the output variables on the individual parameters , $p_1 - p_8$. Table S4 presents the partial correlation coefficients for the outputs on the inputs.

From the partial correlation coefficients in Table S.4, we learn that uncertainties in the exchange time constant between the free troposphere and the boundary layer exert a large influence on the uncertainty in the free tropospheric and marine boundary layer mixing ratios, consistent with their relationship discussed in Section 3.1 of the manuscript. Uncertainties in the stratosphere-troposphere exchange only influence the uncertainties in the mixing ratios of the ozone of stratospheric origins. Uncertainties in the zonal flow and in the ozone loss in the marine boundary layer are of little

importance. Uncertainties in the ozone production rate in the continental boundary layer appear to be of some overall significance.

Table S2: Details of the eight CSTR model input parameters chosen for Monte Carlo uncertainty analysis, together with their 'best estimate' values and units.

Input parameter	Name	Best estimate
$k_{B,m}$	Marine boundary layer decay constant	0.072 day^{-1}
$k_{B,c}$	Continental boundary layer decay constant	1.0 day^{-1}
V_D	Ozone dry deposition velocity over continents [a]	0. 5 cm s^{-1}
STE	Stratosphere-troposphere exchange constant	0.4 ppb day^{-1}
Z_{flow}	Zonal flow velocity	14.5 m s^{-1}
$P_{b,c}$	Continental boundary layer ozone production rate [b]	52.2, 58 ppb day^{-1}
$\tau_{B,i}$	Boundary layer to free troposphere exchange time [c]	2.5, 5.9 days
$\tau_{T,i}$	Free troposphere to boundary layer exchange time [c]	9.4, 37 days

[a] This parameter contributes a linear term; at a given boundary layer height it is subsumed as a constant portion of the continental boundary layer loss constant.

[b] Smaller value is for the Central Asia compartment; larger value is for all other continental boundary layer compartments

[c] Smaller and larger values are for the continental and marine boundary layer compartments, respectively.

Table S3: CSTR model outputs for the 'acceptable' Monte Carlo replicates.

Output		Mean ± 2 – σ confidence limits
Free troposphere	: all O_3	51.7 ± 5.8 ppb
	: stratospheric origins	8.8 ± 4.1 ppb
	: boundary layer origins	42.9 ± 6.3 ppb
Marine boundary layer	: all O_3	37.8 ± 5.2 ppb
	: stratospheric origins	6.7 ± 3.0 ppb
	: boundary layer origins	31.1 ± 5.6 ppb
Tropospheric ozone column density		36.4 ± 3.6 DU
Turnover time		7.2 ± 1.8 days

Table S4: Partial correlation coefficients of the output columns on the input parameter rows in the multiple linear regression analysis of the Monte Carlo replicates.

Parameter	All O_3 FT	All O_3 MB	ST O_3 FT	ST O_3 MB	BL O_3 FT	BL O_3 MB	TOCD, DU	AL, days
$k_{B,m}$	-	-0.16	-0.14	-0.20	0.17	-	0.19	-
$k_{B,c}$	-	-0.27	0.15	-	-0.14	-0.29	0.17	-0.50
V_D	-	-0.11	-	-	-	-0.12	-	-0.23
STE	-	-	0.85	0.87	-0.49	-0.45	-	-
Z_{flow}	-	-	-	-	-	-	-	-
$P_{b,c}$	-	0.26	-0.20	-0.13	0.15	0.31	0.13	-0.91
$\tau_{B,i}$	-	-	0.39	0.42	-0.33	-0.19	-	-0.12
$\tau_{T,i}$	0.22	-0.30	0.53	0.38	-0.14	-0.48	0.15	0.11

Notes:

All O_3: refers to ozone of both stratospheric and boundary layer origins
ST O_3: refers to the mixing ratio of the ozone of stratospheric origins
BL O_3: refers to the mixing ratio of the ozone of continental boundary layer origins
FT: refers to the average over the free troposphere
MB: refers to the average over the marine boundary layer

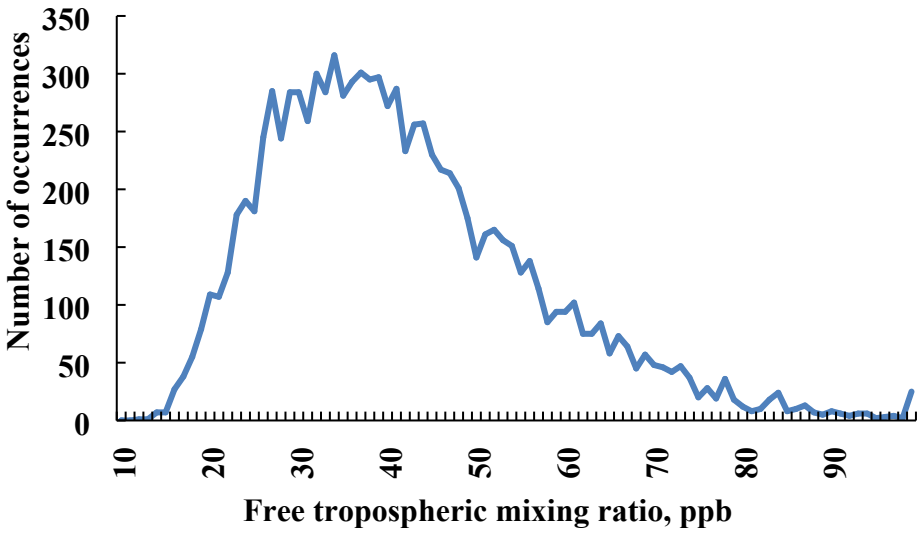

Fig. S11: Frequency distribution of the annual mean free tropospheric ozone mixing ratios calculated by the Monte Carlo replicates.

Section S8: Model simplifications and their likely impact

The 18-compartment model treats ozone sources, loss and transport in an exceedingly simplified manner. In this section we consider the more important simplifications, and discuss their likely impact. In summary, we believe that these simplifications are acceptable, given the purpose for which this model was developed - to provide a simple over-arching explanation of the average seasonal behavior of background tropospheric ozone in the northern midlatitudes.

+ Boundary layer advection ignored. We have included no direct interchange between the boundary compartments. An average west to east flow at these lower altitudes does exist - its average velocity is estimated to be ~2.5 m/s (derived from the NCEP reanalysis for a 30 year annually averaged climatology: https://www.psl.noaa.gov/cgi-bin/data/composites/printpage.pl). In the context of our model this flow would add or dilute ozone to the BL's from the upstream compartment. This additional change becomes important when the upstream compartment has a substantially different (higher or lower) ozone concentration. A case in point is the western MBL compartments where the upstream continental BL compartments have a higher ozone mixing ratio. Model simulations that incorporate boundary layer advection with a flow velocity of 2.5 m/s have been examined. That flow displaces the average marine boundary layer compartment in ~11 days, compared with the 5.9 days average replacement of to the free troposphere compartment. Table S5 summarizes the overall results.

Table S5: Effect of inclusion of MBL advection on model results.

	Base Case	Add MBL advection	Force MBL to 39 ppb
Mean FT O_3 (ppb)	52.15	52.2	52.1
Mean MBL O_3 (ppb)	39.5	40.4	39.4
MBL removal/STE	0.376	0.35	0.376
$k_{B,M}$ (day^{-1})	0.056	0.056	0.062
$k_{B,C}$ (day^{-1})	1.11	1.11	1.11

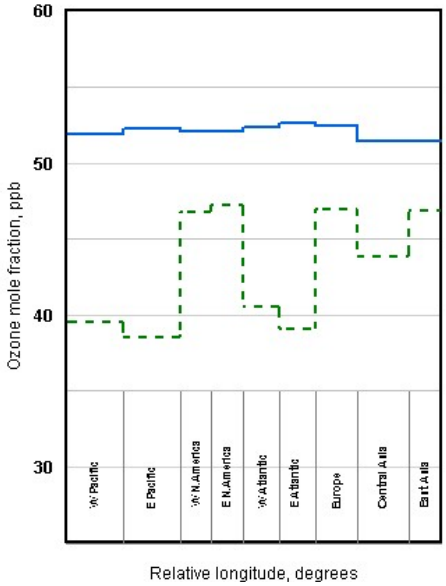

Fig. S12: Simulated annual mean ozone mixing ratios (FT solid blue, BL dashed green) in the 18 model compartments. (Compare to Fig. 2 of the manuscript.)

The second column shows the result of simply adding the BL advection with no change to the inputs. The average marine boundary layer ozone rises by ~1 ppb and the fraction of the total removed by the marine layers decreases slightly. The third column in the Table shows that the original average ozone distribution is closely re-established if the MBL loss rate constant is increased slightly.

The simulation described in the third column of Table S5 would change Fig. 3 of the paper to that shown in Figure S12. The infusion of ozone by flow from the continents creates a negative gradient across the

oceans, as expected. Conversely, the inflow of cleaner air from the Pacific results in a small positive gradient in the continental BL across North America.

The effect of MBL zonal flow on the seasonal ozone behavior is shown in Figure S13. The left-hand panel is a copy of Figure 8b in the text. The right-hand panel results from the introduction of 2.5 m s^{-1} zonal MBL flow and a small increase in the MBL loss constant from 0.053 to 0.061 day^{-1}. The two panels are thus a similar comparison to that in the steady state runs represented in the first and third columns of Table S5 above. Little difference is introduced in the overall seasonal dependences. The most visible effect is a separation of the MBL curves (blue) into two sets of two curves - the lower two being those for the eastern segments of the oceans - caused by the gradient across the oceans noted above. The difference between the two segments (east vs. west) of each ocean maximizes in the summer. Overall, inclusion of MBL zonal flow does not alter any conclusions of the paper.

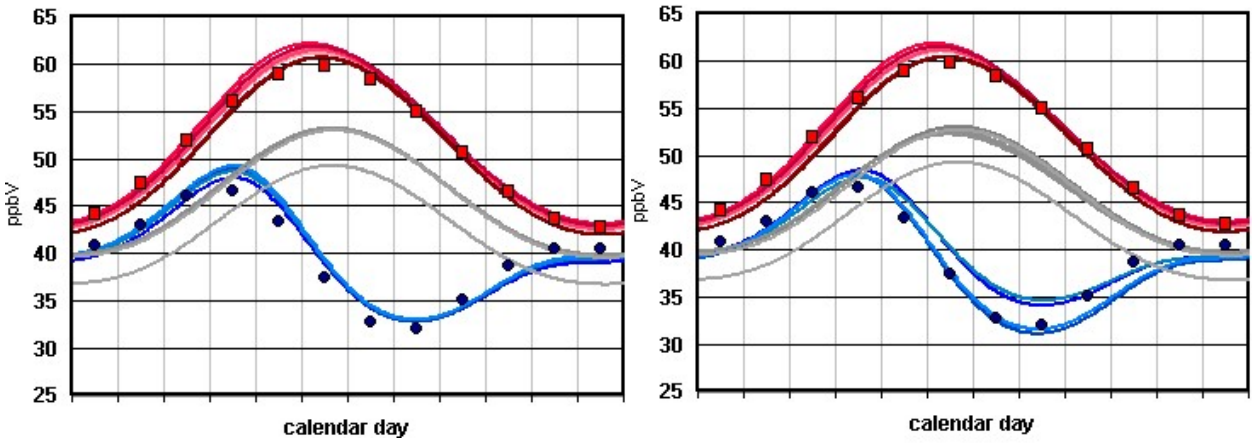

Fig. S13: Simulated seasonal dependence with no BL intercompartment flow as in Fig. 8b of text (left) compared with 2.5 m/s flow and kB,m raised from 0.053 to 0.061 d^{-1} (right). Upper (red) and lower (blue) curves indicate FT and MBL compartments, respectively, with continental BL compartments in the middle (grey); Central Asia is the outlier. Observed seasonal cycles for the MBL at Mace Head (blue circles) and the FT from European alpine sites (red squares) are shown for comparison. On the right, the MBL curve in closest agreement with the Mace Head data is the eastern Atlantic segment, which contains the Mace Head site.

+ Surface deposition ignored. We attribute ozone losses in both the MBL and CBL compartments to a global first order process with a global first order "rate coefficient". In the real atmosphere this is a complex system with both gas phase photochemical and heterogeneous processes, including surface deposition. This paper does not propose to derive the correct functional form of these rate coefficients from the underlying physical and chemical processes. Instead, their magnitude and their seasonal behavior are constrained by the required matching of the available data and overall mass balance. However, where instructive, simple derivations using available data are presented.

Marine boundary layer: We used two methods to inform the marine boundary layer rate coefficient: (1) the simple first principles derivation based on the $O(^1D) + H_2O$ photochemical mechanism described in

Supplement S1 and (2) a mass balance argument based on the measured seasonal ozone cycles in Supplement S2. The two methods yielded similar functional forms for their seasonal behavior, and the simple O^1D derivation produced an average value similar to that needed to fit the measured data, given our assumed boundary layer height and mixing behavior. The possible contribution of surface deposition to this evaluated rate coefficient is made using a recommended value for the deposition velocity $V_{d,m}$ from the ATom results (J. Peischl, 2022, private communication) of 0.018 cm/s. For our 1000m height, this process would clean the boundary layer in ~64 days, corresponding to a first order rate coefficient of 0.015 d^{-1}, a value equal to ~1/4 of the base case value of $k_{B,m}$ (0.056 d^{-1}) reported in Table 1 of the manuscript.

Continental boundary layer: A similar reasoning holds for the continents. Estimates of 0.4 cm/s for $V_{d,c}$ (Clifton et al., 2020) give a clearance time of 4.3 days for our 1500m boundary layer, or a contribution to the overall rate coefficient of 0.23 d^{-1}, again roughly ~1/4 of our typical global values near 1 d^{-1}.

These deposition processes are therefore minor, but do account for significant portions of the ozone losses in the continental BL. Investigation of the details of the boundary layer loss processes is outside the scope of this paper however, and being naturally first order, they are subsumed in the global rate coefficients in the model. Overall mass balance does place mutual constraints on the related processes of photochemical production, photochemical loss and surface deposition, which can be useful at the next level of complexity. For instance, using the parameter values and results for the base case in Table 1 and Figure 3, a value of 0. 4 cm/s for $V_{d,c}$ would require a net photochemical ozone production of 9.0 ppb/d in the continental boundary layer, whereas a much lower value of $V_{d,c}$ of 0. 07 cm/s would be required if net photochemical production were zero (i.e., photochemical production and loss were balanced. An intermediate value of 0.15 cm/s would require a net photochemical production of 2 ppb/d, in rough agreement with more complex models (e.g., Crutzen et al., 1999). Thus, the joint restraints placed on these connected parameters by the overall mass balance can be used to bracket and optimize the parameter values.

+ Incomplete treatment of MBL ozone loss. Section S1 and S2 detail the treatment of MBL ozone loss that is triggered by JO(^{1}D) photolysis of ozone, and subsequent reaction of O(^{1}D) with water vapor. This treatment includes multiple omissions and simplifications, including:

- ***Seasonal cycle of stratospheric ozone column ignored*.** JO(^{1}D) photolysis of ozone depends strongly on the seasonal variation of stratospheric ozone column. Figure S14 shows that seasonal variation as determined by satellite measurements; the peak-to-peak variation in monthly means is ± 12%.
- ***Variation in Cloudiness ignored:*** There are indications that Cape Grim, where Wilson, 2015 measured the

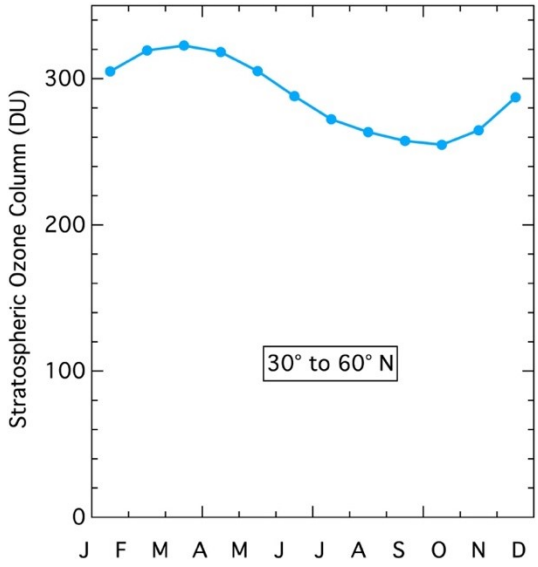

Fig. S14: Seasonal cycle of the stratospheric ozone column at northern mid latitudes (Ziemke et al., 2011).

seasonal dependence of $J(O^1D)$, is significantly less cloudy than typical mid-latitude MBLs. Satellite determinations suggest mean annual cloud cover (Fig. S15) at Cape Grim is ~68%, but mid-latitude marine regions appear to be nearer 80%.

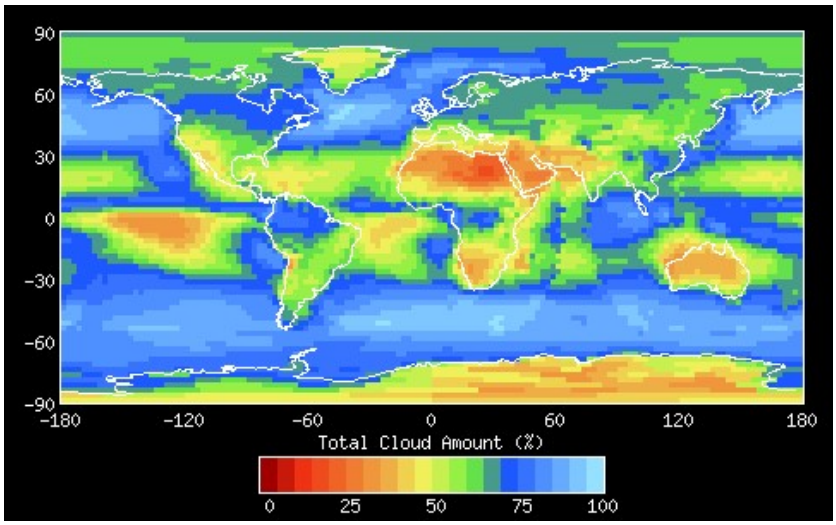

Figure S15: Mean annual cloud cover from ISCCP July, 1985-December, 2009. (https://isccp.giss.nasa.gov/products/browsed2.html)

In addition to the two issues discussed above, there is possibly important complexity in MBL ozone photochemistry; $JO(^1D)$ photolysis of ozone triggers a manifold of HOx and possibly halogen reactions that not only can enhance ozone destruction, but also can lead to ozone production depending upon the abundance of NO_X. As discussed above for surface deposition, this paper does not intend to derive the correct functional form or magnitude of MBL ozone loss from the underlying physical and chemical processes. Instead, its magnitude and seasonal dependence are constrained by the required matching of the available data and overall mass balance. Section S1 and S2 present instructive, simple derivations using available observations.

+ FT photochemistry ignored. We note that both photochemical production, $P(O_3)$, and loss, $L(O_3)$, of ozone each make large contributions to the ozone budgets in the FT compartments, but these quantities are difficult to parameterize and are in close balance globally; thus we omit any treatment of these processes. The impact of $P(O_3)$ within the MBL is also omitted. The recently-available photochemical climatology developed from the ATom data set (Guo et al., 2021) gives a basis for an evaluation of the impact of these omissions. Examination of the estimates of $P(O_3)$ vs. $L(O_3)$ for all the Northern Hemisphere midlatitude legs over the oceans allows for a quantification of the net ozone production in the remote troposphere. Using 10 s (~2 km) airborne measurements from four flight missions (one from each season) the ATom science team produced a reactivity data stream that ran each parcel's ozone concentration out to a diel steady-state so that an accurate daily and in totum annual ozone photochemical reactivity could be obtained. Analyzing only the data flown over the Northern midlatitude oceans we found that the Pearson correlation coefficient between production and loss was 0.5. Figure S16 shows the average net (P-L) ozone photochemical rates in 500 m altitude bins from the MBL up to 12 km (approximately the upper 220 hPa bound of this work's model) and then makes an air density weighted average for the marine FT and the MBL. As assumed at the outset of this modeling exercise the effective (net) photochemical lifetime of ozone in the free troposphere is ~3.5 years (52 ppb/0.04 ppb d^{-1}) much longer than zonal and vertical mixing making the free troposphere an effective long-lived reservoir of global ozone.

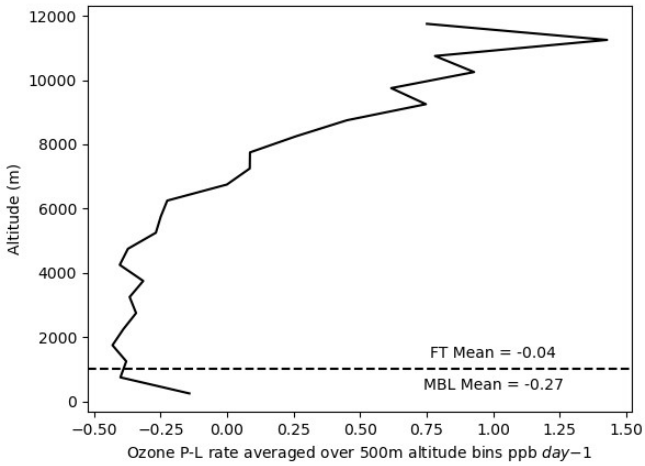

Figure S16: Mean net (P-L) ozone photochemical production rates at northern midlatitudes in 500 m altitude bins calculated from the ATom data set (Guo et al., 2021).

+ Assumption of a well-mixed free troposphere: The idea that the free troposphere over the northern midlatitudes can be thought of as a well-mixed reservoir came to us originally from the simple consideration that the ozone lifetime in the free troposphere is long with respect to circum-global transport times – hence the well-mixed picture must be valid, as discussed in more detail by Parrish et al. (2021). Indeed, it was this idea that led us to develop our model, rather than being revealed by the model results. We have since learned that we were not the first to reach this realization; Junge (1962) had this idea ~40 years earlier. We expanded the introduction to the model description to clarify this issue.

When considering variability in mean FT ozone we do acknowledge in our paper that a vertical gradient exists in accord with a natural source from the stratosphere aloft and a sink at the surface. This gradient is on average ~1.5 ppb/km in the bulk of the FT, and therefore ozone routinely increases by ~15 ppb across the depth of the troposphere. Therefore, when evaluating differences in observed free-tropospheric ozone, it is important to compare averages of profiles through the FT and, not include the vertical variation in an estimated "range" of observed FT ozone.

Parrish et al. (2020) tested the well-mixed reservoir idea through examination of vertical profiles of baseline ozone from the surface up through the mid-free troposphere at the west coasts of North America and Europe. They found no statistically significant differences between the data sets in either the annual mean vertical profile (see their Fig. 5) or the seasonal cycle (see their discussion of Figs. 6 and 7; note that, as discussed by Parrish et al. (2020), the somewhat larger annual mean ozone from the European sonde data at high altitudes in Fig. 5 is believed to be a measurement issue with the sonde data). Our goal in that paper was to quantify the degree of zonal similarity; a high degree of similarity was indeed found.

In summary, to the best of our knowledge, all recent examinations of northern midlatitude ozone measurements agree with our concept that ozone in the free troposphere at northern midlatitudes is accurately described as a “well-mixed reservoir” (with the acknowledged averaging over the vertical gradient).

+ Assumption of first order ozone destruction kinetics: For the mechanistic kineticist, this is an enormous simplification. We do acknowledge the non-linear kinetics that result from the complex mechanisms of ozone formation and destruction. According to global budgets of tropospheric ozone estimated by more complex models (e.g. Hu et al., 2017) the largest sinks are in fact first-order; namely, photolysis (responsible for about half of the photochemical terms) and dry deposition. Furthermore, outside of net production regions, because their losses are quadratic by nature, the abundance of HOx is primarily proportional to the square root of ozone (the main source.) Therefore, the odd oxygen mediated losses will tend to not deviate strongly from a linear dependence.

More germane to the issue of the fidelity of our model, any 2nd order character of the loss processes would not cause a problem within the model. The loss processes serve to balance the production terms at specified mean ozone concentrations in the MBL and FT. It is convenient, and approximately correct, to represent those loss terms as first order in ozone; however, including a more complex description of the loss processes would not change the production vs. loss balance. A more complex treatment of the loss processes could possibly affect the ozone concentration in the CBL, but the comparison of our model results with observations (Fig. 9) suggests that this simplification does not add large uncertainty to our model results.

+ Assumption of no ozone all photochemistry in the FT: The model assumes that none of the ozone photochemical production or loss occurs in the FT; all of the production is assigned to the continental BL, along with all of the photochemical loss, except for the fraction that occurs in the MBL. Figure S17 shows the changes in the model results that come from assigning a fraction of the photochemical production to the free troposphere. To maintain zero net ozone production in the FT, a parallel fraction of the photochemical ozone destruction must also move to the FT, with less remaining in the continental BL. Since the ozone concentrations are constrained in the model, the concentrations in all model compartments remain constant; what does change is that the derived first-order loss rate coefficient, $k_{B,c}$, for the continental BL decreases (Fig. S17a) and the FT and STE sources of ozone to the continental BL increase (Fig. S17b). We have not attempted to determine the correct value for this fraction, either from observations or more complex model calculations. This is an issue that could be investigated in future work.

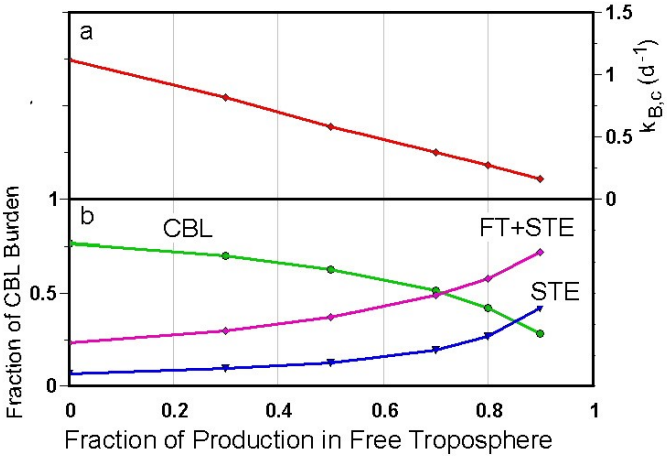

Figure S17: Dependence of (a) the continental BL first-order loss rate coefficient, $k_{B,c}$, and (b) the sources of continental BL ozone as a function of the fraction of ozone photo-chemical production assigned to the FT.

Section S9: Examples of the use of simple models in complex investigations:

In our view, the primary utility of our model is providing the reader/researcher with a mental picture on which to base evaluation of published literature and the reader's own measurement or modeling results. The centrality of models / mental pictures in the progress of science - in this case climate models - was elegantly described by Held[4] . Quotes from this work are reproduced here: "On the one hand, we try to ***simulate*** by capturing as much of the dynamics as we can in comprehensive numerical models. On the other hand, we try to ***understand*** by simplifying and capturing the essence of a phenomenon in idealized models, or even with qualitative pictures" Further, "As our comprehensive models improve, they more and more become the primary tools by which theory confronts observations." But he adds "… we typically gain understanding of a complex system by relating its behavior to that of other, especially simpler, systems." After describing the value of holistic understanding of some of the component processes in the climate, such as deep convection schemes and boundary layer models, he makes this statement: "An elegant model is only as elaborate as it needs to be to capture the essence of a particular source of complexity, but is no more elaborate." and "Elegance and lasting value are correlated." It is these pictures that will last. They can guide the advances in the complex models as they become more and more complex and better in their simulation of nature and they are the connections that can best gain understanding of the differences between models. As such, the simple models should be pursued and used simultaneously with measurements and more complex simulations. We hope that this paper will trigger such uses by the community. We believe incorporation of the schematic model that we present into a scientist's basic understanding of the tropospheric ozone budget will be beneficial in the development of better complex models and inform those results.

The "use" of the model in this paper is to provide a concise, elegant, explanation for the average (climatic) seasonal behavior of northern midlatitude ozone and illustrate the governing influence of the marine boundary layer on this averaged (climatic) behavior. Two components of the simple picture are critical to the understanding gained. First, in the marine boundary layers ozone is removed predominantly via the O^1D channel at rates that, with any reasonable mixing reproduces the observed amounts and seasonal behavior. Second, the picture of a well-mixed free troposphere, from which the MBL receives most of its ozone, produces longitudinal similarity observed in the free troposphere and the marine boundary layers. These two central features of the model are not new of course, but this particular use is. We acknowledge the considerable approximations in this model in the section above. Despite the simplifications, the seasonal behavior of the marine boundary layer and the free troposphere is well reproduced and we believe strongly support the model we present for that purpose.

The current model illuminates other aspects, implying further utility:

Constraints on continental production: A further use of the model is actually subsumed in the text. We show how, given the requirements to match the FT and MBL behavior along with the need for mass balance actually confines the net contributions of continental BLs. For a given set of parameters, this produces a prediction of continental BL ozone concentrations shown in Figure 9 of the text, where approximate agreement with the CASTNET data is encouraging. Expansion of the model to distinguish the longitudinal segments would be instructive.

Estimates of regional background ozone: Regional models require an estimate of the background ozone to which regional sources are added. Our model has substantial background ozone arriving by down-mixing from the free troposphere reservoir. For the parameter set used for Figure 8b approximately 25% of the continental ozone burden is supplied by down-mixing of FT ozone, which has contributions from photochemical from all of the other continental segments as well as from STE. This contribution provides an estimates of the background ozone at regional continental surface sites. Figure S17 shows how this contribution varies with the fraction of total ozone production assumed to occur in the FT. If this fraction rises to 90%, then approximately 75% of the continental ozone burden would be supplied by down-mixing of FT ozone.

Generation of parameters by averaging of complex model results: Suitable averages of the results of complex simulations can produce the effective simple parameters to compare with those in our model. Examples include (1) the first order rate coefficients and how good is first order behavior? (2) the seasonal behavior boundary layer structure and ventilation rates. Such mutual exercises will show contrasts between the models, likely could inform the source of those differences. Simultaneous improvement of both models are expected.

"Reality checks" in the evaluation of complex data: The ability for measurement and modeling of the atmosphere in ever-increasing detail points to a key use for simpler models. The over-arching constraints of the planetary atmosphere and mass balance must be obeyed by the more complex data when suitably averaged.

It is not the purpose of this paper to criticize published literature, but it is our observation that the atmospheric chemistry literature contains papers in which complex model results or detailed measurements would have benefited by reference to the simpler picture of the atmosphere and avoided what we believe are erroneous conclusions. Consultation with the understading in the simple model: Two examples: (1) The model and its simple mass balance shows that marine boundary losses must total ~2ppb/day with any reasonable FT-MBL mixing intensity. Some recent reports indicate values an order of magnitude lower. (2) The model with its mixed FT reservoir requires zonal similarities between northern midlatitude regions observed or simulated in other studies. Yet there are published examples with FT ozone showing marked zonal differences - inconsistent with the simple model. Consideration of these results from the perspective of the mental picture provided by the simple model could have led to deeper investigation of such inconsistent results.

Use of simple models as a guide: Specific uses of this "tool" can be forward looking, prompting questions to be gleaned from the measurements and models. We have raised some: for example, how closely does a first order destruction rate coefficient in the continental boundary layer fit the detailed data?, and how does it diverge due to a departure from our assumed first order loss? What is the seasonal cycle of ventilation of the boundary layers?. Do the related and competing effects of boundary layer height and convective mixing intensity produce a BL mixing "ventilation" time that varies significantly with season or do they largely cancel? We expect some revealing results to emerge when such analyses are performed, prompted by such questions.

References:

Ayers, G. P., H. Granek and R. Boers *(*1997), Ozone in the marine boundary Layer at Cape Grim: model simulation, *J. Atmos. Chem.,* 27, 179–195.

Ayers, G. P., and I. E. Galbally (1995), A preliminary estimation of boundary-layer-free troposphere entrainment velocity at Cape Grim, in A. C. Dick and J. L. Gras (eds), *Baseline 92*, Bureau of Meteorology, Australia, pp. 10–15.

Boyin, H., P. W. Thorne, V. F. Banzon, T. Boyer, G. Chepurin, J. H. Lawrimore, M. J. Menne, T. M. Smith, R. S. Vose, and H.-M. Zhang (2017), Extended Reconstructed sea surface temperature, Version 5 (ERSSTv5): Upgrades, validations, and intercomparisons, *J. Climate,* 30, 8179-8205. doi.org/10.1175/JCLI-D-16-0836.1.

Burkholder, J. B., S. P. Sander, J. Abbatt, J. R. Barker, C. Cappa, J. D. Crounse, T. S. Dibble, R. E. Huie, C. E. Kolb, M. J. Kurylo, V. L. Orkin, C. J. Percival, D. M. Wilmouth and P. H. Wine (2019), Chemical Kinetics and Photochemical Data for Use in Atmospheric Studies, Evaluation No. 19," JPL Publication 19-5, Jet Propulsion Laboratory, Pasadena, http://jpldataeval.jpl.nasa.gov.

Clifton, O. E., A. M. Fiore, W. J. Massman, C. B. Baublitz, M. Coyle, L. Emberson, S. Fares et al. (2020), Dry deposition of ozone over land: processes, measurement, and modeling, *Rev. Geophys.,* 58(1), e2019RG000670.

Crutzen, P. J., M. G. Lawrence and U Põschl (1999), On the background photochemistry of tropospheric ozone, *Tellus,* 51A-B, 123–146.

Gaudel, A., et al. (2020). Aircraft observations since the 1990s reveal increases of tropospheric ozone at multiple locations across the Northern Hemisphere, *Sci. Adv., 6*, eaba8272.

GISTEMP Team (2021): *GISS Surface Temperature Analysis (GISTEMP), version 4*. NASA Goddard Institute for Space Studies. Dataset (ersst.1971-2020.climatology) accessed 2021-10-09 at https://data.giss.nasa.gov/gistemp/

Guo, H., et al. (2021), Heterogeneity and chemical reactivity of the remote troposphere defined by aircraft measurements , *Atmos. Chem. Phys.,* 21, 13729–13746, https://doi.org/10.5194/acp-21-13729-2021.

Hu, L., et al. (2017), Global budget of tropospheric ozone: Evaluating recent model advances with satellite (OMI), aircraft (IAGOS), and ozonesonde observations, *Atmospheric Environment, 167*, 323e334.

Junge, C. E. (1962), Global ozone budget and exchange between stratosphere and troposphere, *Tellus*, XIV, 363-377.

Kerr, G. H., D. W. Waugh, S. D. Steenrod, S. A. Strode and S. E. Strahan (2020), Surface Ozone-Meteorology Relationships: Spatial Variations and the Role of the Jet Stream. *J. Geophys. Res.*, *125*(21), e2020JD032735.

Lelieveld, J., and F.J. Dentener (2000), What controls tropospheric ozone? *J. Geophys. Res.,* 105, 3531-3551.

Lenssen, N., G. Schmidt, J. Hansen, M. Menne, A. Persin, R. Ruedy, and D. Zyss (2019), Improvements in the GISTEMP uncertainty model. *J. Geophys. Res. Atmos.*, 124, 12, 6307-6326, doi:10.1029/2018JD029522.

Parrish, D. D., et al. (2016), Seasonal cycles of O_3 in the marine boundary layer: Observation and model simulation comparisons, *J. Geophys. Res. Atmos., 121*, 538–557, doi:10.1002/2015JD024101.

Parrish, D.D., R.G. Derwent, S. O'Doherty, and P.G. Simmonds (2019), Flexible approach for quantifying average long-term changes and seasonal cycles of tropospheric trace species, *Atmos. Meas. Tech.*, *12*, 3383–3394, https://doi.org/10.5194/amt-12-3383-2019.

Parrish, D. D., R. G. Derwent, W. Steinbrecht, R. Stübi, R. Van Malderen, M. Steinbacher, et al. (2020), Zonal similarity of long-term changes and seasonal cycles of baseline ozone at northern mid-latitudes. *J. Geophys. Res.: Atmos., 125*, e2019JD031908, https://doi.org/10.1029/2019JD031908 doi: 10.1029/2019JD031908.

Parrish, D. D., R. G. Derwent and I. C. Faloona (2021), Long-term baseline ozone changes in the Western US: A synthesis of analyses, *J. Air & Waste Manage. Assoc.,* 71:11, 1397-1406, DOI: 10.1080/10962247.2021.1945706.

Wilson, S. R., Characterisation of J(O1D) at Cape Grim 2000–2005 (2015), *Atmos. Chem. Phys.*, 15, 7337–7349, doi:10.5194/acp-15-7337-2015.

Ziemke, J.R., S. Chandra, G.J. Labow, P.K. Bhartia, L. Froidevaux and J.C. Witte (2011), A global climatology of tropospheric and stratospheric ozone derived from AURA OMI and MLS measurements, *Atmos. Chem. Phys.,* 11, 9237-9251.